

See discussions, stats, and author profiles for this publication at: <https://www.researchgate.net/publication/266085715>

Fabrication of a Superhydrophobic Al₂O₃ Surface Using Picosecond Laser Pulses

ARTICLE *in* LANGMUIR · SEPTEMBER 2014

Impact Factor: 4.46 · DOI: 10.1021/la5033527 · Source: PubMed

CITATIONS

4

READS

58

1 AUTHOR:



Radhakrishnan Jagdheesh

Universidad Politécnica de Madrid

23 PUBLICATIONS 67 CITATIONS

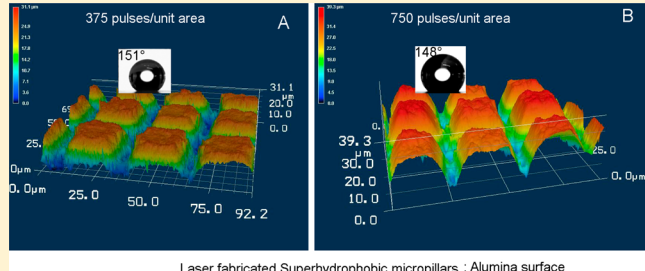
[SEE PROFILE](#)

Fabrication of a Superhydrophobic Al_2O_3 Surface Using Picosecond Laser Pulses

R. Jagdheesh*

School of Mechanical and Manufacturing Engineering, The University of New South Wales, Sydney NSW 2052, Australia

ABSTRACT: Ultrashort pulse laser (USPL) machining/structuring is a promising technique to create a micropattern on a material surface with very low distortion to the peripheral area or high precession. Thin sheets of alumina (Al_2O_3) are micromachined with ultraviolet laser pulses of 6.7 ps, to create a superhydrophobic surface by single-step processing. USPL patterned micropillars and microholes have been fabricated with a range of pulses varying from 100 to 1200 pulses/unit area. The impact of the number of pulses/unit area with respect to the geometry and static contact angle measurements has been studied. The surface is free from cracks, and the melting effect is well-pronounced for the blind microhole structures. An energy dispersive X-ray spectroscopy study revealed a marginal change in the elemental composition of the laser-patterned surface. The results show that the geometry of the laser-machined pattern plays a major role in changing the wetting properties rather than the chemical changes induced on the surface. The micropillars exhibited a consistent superhydrophobic surface with a static contact angle measurement of $150^\circ \pm 3^\circ$.



Laser fabricated Superhydrophobic micropillars : Alumina surface

1. INTRODUCTION

Ultrafast laser sources are used for ablating a wide range of materials^{1–3} due to their ability to fabricate micro/nanoscale features with very limited distortion to the peripheral area. Material is removed from a substrate by ablating the surface, using one or more laser pulses. The ablation process, and thus the micron-scale features created, depends on the laser properties, such as laser pulsedwidth, energy of the pulse, repetition rate, and the material used.

Surface morphology is a prime factor determining the wettability of a solid surface. The wettability of a solid surface is normally addressed by measuring the static contact angle measured between the water droplet and the solid surface. In general, a hydrophilic surface has a contact angle of less than 90° and a hydrophobic surface of more than 90° . Superhydrophobic surfaces have a contact angle of more than 150° .⁴

The wettability of the solid surface mainly depends on two factors: surface topology and chemistry.^{5,6} Hydrophobic surfaces have attracted much attention due to their potential applications in microfluidics, in lab on chip devices, and as functional surfaces for the aerospace and automotive industries. Patterning is the one of the effective ways to change the topography and improve the wetting property of the metal surface.

In recent years, inspired by the topography of the lotus leaf, numerous methods like plasma surface modification, radiation grafting, various coatings methods, electrochemical deposition, electroless replacement deposition, lithographically patterned substrates, vertically aligned carbon nanotubes, nanocasting and extruding of polymers, natural oxidation, and laser patterning have been adopted for development of hydrophobic surfaces.^{7–13} Among the surface modification techniques

available, laser patterning is a unique technique that can modify the topology with very minimum thermal distortion to the bulk material. Moreover, it is a noncontact, very precise method, and complex patterns can be fabricated on the surface. The nanoscale ripples found on the laser-patterned surface are commonly known as laser-induced periodic surface structure (LIPSS), which can be observed near the ablation threshold. In most cases, the orientation of the regular ripples are found to be perpendicular to the polarization direction of incident laser beam.⁶

Successful attempts were made by Baldacchini et al. to convert a hydrophilic silicon surface to hydrophobic by applying a fluorosilane coating on laser-textured surface.¹⁴ The transformation of a surface from hydrophilic to hydrophobic was also recorded without additional coating on the surface after laser treatment.¹⁵ The transformation of wetting property from hydrophilic to hydrophobic was reported by Bhattacharya et al. on hydrophobic clustered-copper nanowires without using any low surface energy material coating. The transition was purely a geometrical phenomenon related to the nature of clustering.¹⁶ Kietzig et al. studied the time dependency of hydrophobicity on the structure created by femtosecond laser machining on different metals and alloys. They observed that the laser-induced dual scale roughness structures play a significant role in the wetting properties of the metal surfaces.¹⁷ Wu et al. showed that surfaces with double scale structure showed higher static contact angle.¹⁸

Received: August 21, 2014

Revised: September 8, 2014

Published: September 24, 2014



Table 1. Laser-Processing Parameters

laser wavelength (nm)	laser power (mW)	laser repetition rate (kHz)	pitch (μm)	energy/pulse (μJ)	fluence (J/cm^2)	apparent spot diameter (μm)	number of pulses/unit area
343	1000	200	20	5	2.82	15	100–1200

The hydrophobicity of solid surfaces follows either the Cassie–Baxter model¹⁹ or the Wenzel model.⁵ According to Wenzel's model, the liquid is in contact with the whole surface and the hydrophobicity of a solid surface is improved by an increase in solid/liquid interfacial area due to the surface roughness. For the Cassie–Baxter model, the surface has voids in geometrical structures, where air can be trapped and the liquid cannot penetrate. In this case, instead of a solid/liquid interface, it has solid/liquid and liquid/vapor interface. Therefore, if the surface roughness has regular patterns of square or conical protrusions (pillars), air can be trapped inside the valleys, and it follows the Cassie–Baxter model.

Ultrashort pulse laser (USPL) machining/structuring is a promising technique to obtain a micropattern on a material surface. In the recent past, an USPL has been used to micromachine ceramics.²⁰ It is very difficult to create micro/nanostructures on a brittle ceramic substrate to transform the wetting properties. Application of conventional techniques to micromachine the ceramic surface is limited due to the cracking and deformation of the structures. There are no scientific reports on the microfabrication of Al_2O_3 with a direct laser-writing technique for improving the wetting properties, to the best of our knowledge. Therefore, an attempt has been made to create a superhydrophobic surface in a single step by altering a material's surface structures with a picosecond laser source.

In this paper, we investigate the development of a superhydrophobic surface on flat alumina (Al_2O_3) sheets using a direct laser-writing technique. Two different geometries, such as blind microholes and micropillars, have been patterned on the substrate to achieve the superhydrophobicity. The surface structure has been analyzed with scanning electron microscopy (SEM) and confocal laser scanning microscopy (CLSM). The improvement in the wetting properties was evaluated with static contact angle measurements using the sessile drop technique.

2. EXPERIMENTAL SECTION

Flat alumina (Al_2O_3) plates were laser-machined by ultraviolet laser pulses with different laser process parameters. Samples with the size of $10 \times 10 \times 1 \text{ mm}^3$ were used for the laser-patterning experiments. A frequency-tripled (wavelength 343 nm) Nd:YAG laser with an average power of 15 W was used for this experiment. The application of laser pulses with shorter wavelength allows smaller diffraction-limited spot sizes and therefore fine features in the patterned surface. The experiments were performed at a fixed pulse duration of 6.7 ps. The linearly polarized laser beam was guided over the samples by a two-mirror Galvo scanner system, and the angle of incidence was fixed at 90° onto the targets. The laser beam has a Gaussian energy density profile. Microfeatures were fabricated with an apparent spot size of 15 μm . Laser-machining was performed in a semiclean room at atmospheric conditions. The best-suited laser-processing parameters with respect to the hydrophobicity were selected by experimenting with different laser powers and the number of pulses/unit area. The samples were cleaned with acetone prior to laser-machining. The detailed laser-processing conditions are shown in Table 1.

The microfeatures of laser-machined samples were analyzed by scanning electron microscopy (SEM), with energy dispersive X-ray spectroscopy (HITACHI, model S-3000N) and confocal laser scanning microscopy (CLSM) used to evaluate the microstructure

and the geometry of the microchannels. Energy dispersive X-ray spectroscopy (EDS) measurements were made to evaluate the chemical changes on the laser-patterned surface. The hydrophobicity/water repellency of the samples was studied by measuring the static contact angle using the sessile drop technique, with a video-based optical contact angle measuring device (OCA 15 plus from Data Physics Instruments). An 8 μL droplet of distilled deionized water was dispensed on the laser-machined surface structures under atmospheric conditions, and the static contact angle was calculated by analyzing droplet images recorded just after the drop deposition.

3. RESULTS

Primarily, it is essential to understand the geometry or the shape of the micropatterns with respect to the static contact angle (SCA) measurements. Two different micropatterns, such as micropillars and blind microholes, have been fabricated for different laser parameters, particularly by changing the number of the laser pulses applied to the unit area. The pitch of the laser beam has been fixed at 20 μm (the distance between successive laser tracks). An increase in the number of applied laser pulses would change the depth of the micropatterns. All the laser-machined samples exhibited a hydrophilic property immediately after the laser fabrication process. Figure 1

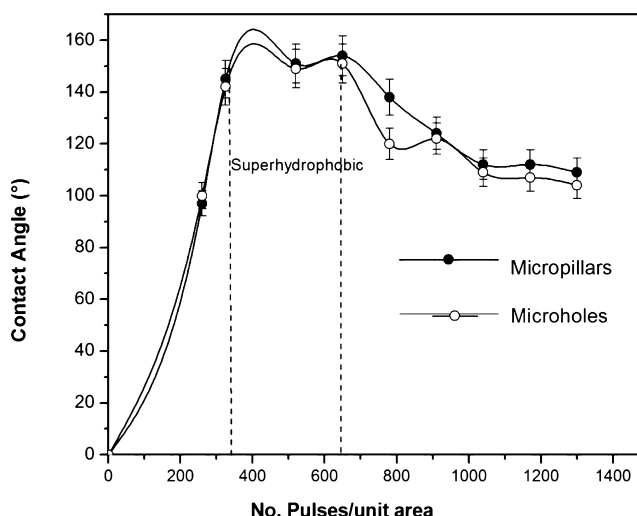


Figure 1. Static contact angle measurements with respect to the number of laser pulses/unit area.

represents a summary of SCA measurements as a function of pulses/unit area on blind microholes and micropillars measured after 72 h from the time of fabrication. The samples processed with laser pulses between 375 and 750 pulses exhibited a superhydrophobic property. The results clearly suggest that the superhydrophobic surface can be achieved with a definite width and height of the microfeatures fabricated. The detailed results and discussion about the micropattern and the wetting properties have been limited to those samples.

The micropillars have been fabricated by scanning the Al_2O_3 flat surface in X and Y directions with a horizontal displacement of 20 μm between successive laser tracks/scans. However, the uniform depth of the channels in the X and Y directions is

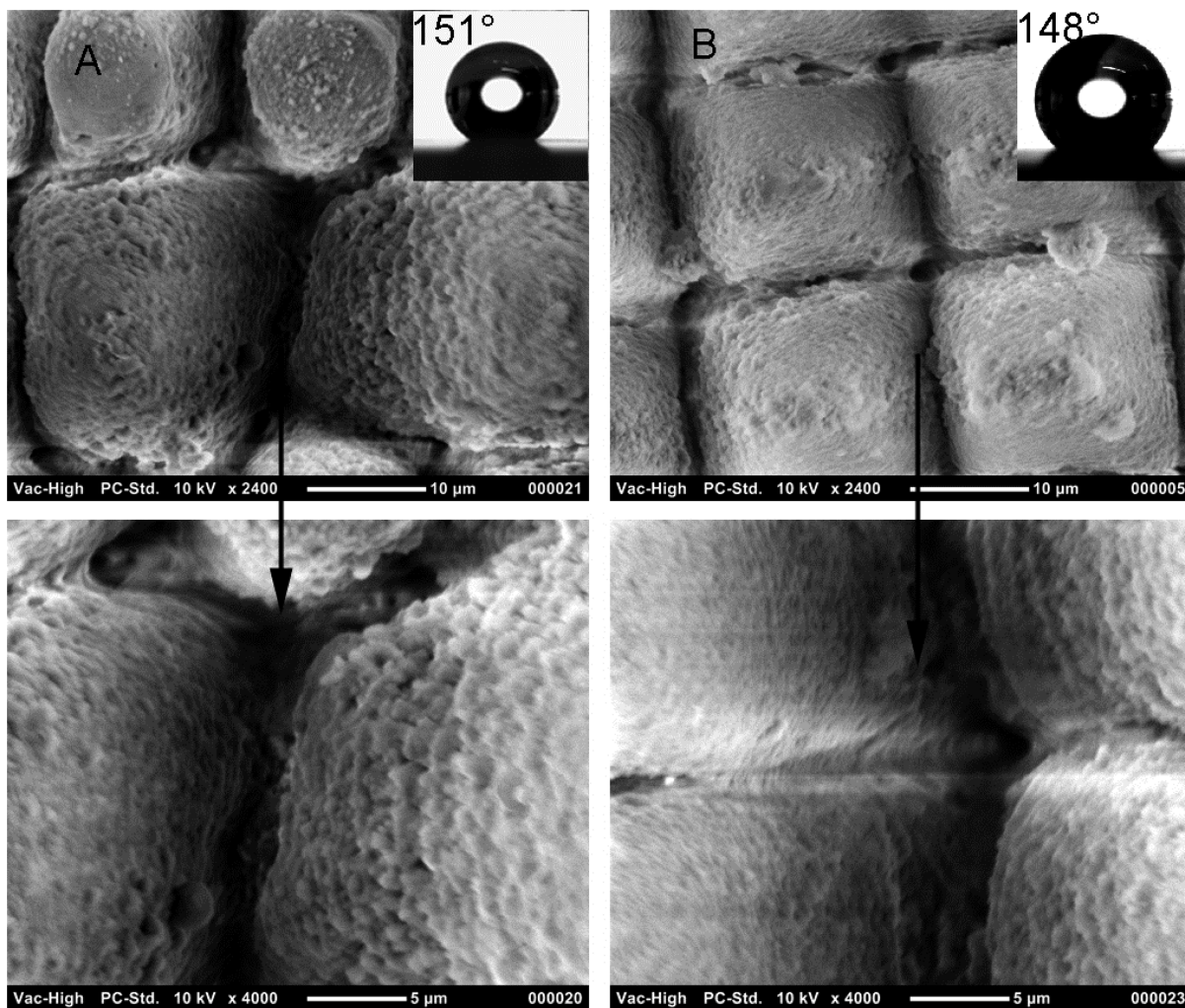


Figure 2. SEM pictures of laser micropillars: (A) 375 pulses/unit area and (B) 750 pulses/unit area.

achieved by having an overlap of more than 98% pulse to pulse along the laser-scanning direction. Figure 2 shows the micropillars fabricated with 375 and 750 pulses/unit area. The difference in applied laser pulses has resulted in an increase in channel depth or height of the micropillars. The hydrophobic property starts deteriorating as the distance between the micropillars is above 6 μm . The microstructure is clean and there is no presence of debris or resolidified material vapor. The micropillars fabricated with 375 pulses/unit area show the signature of clear ablation. Further, the cascaded nanoscale protrusion found on the walls of the micropillars shows the layer-by-layer removal of the material. The kind of ripple structure normally found after laser ablation⁶ of a metal surface is absent in this case.

The micropillars fabricated with 750 pulses/unit area show finer surface structures compared to the micropillars fabricated by 375 pulses/unit area. The reason could be related to more heat being applied to the same spot by increasing the number of pulses/unit area. This may increase the localized temperature and improve the ablation efficiency. The higher magnification image of the bottom of the micropillars (intersecting point of the X and Y directions) shows the near disappearance of the nanoscale protrusions.

Further, the micropillars prepared with 750 pulses/unit area show signs of melting. This is very clear in comparing the

magnified SEM pictures of the sample prepared with 375 and 750 pulses/unit area. This ablation patterns observed in the picosecond laser fabrication are quite comparable with the structures reported for the laser ablation of Al_2O_3 with femtosecond laser pulses.²⁰

Figure 3 show the SEM pictures of the blind microholes generated by laser processing. Two sets of blind microholes with the laser-scanning distance of 20 and 50 μm have been produced. The distance has been changed to avoid the hump build up around the circumference of the blind microholes. The holes are processed with 375 pulses/unit area. It is very clear from the higher magnified image of the blind microholes that the top edge shows the signature of layer-by-layer material removal from the ablated region. However, the inner wall of the holes shows the material melting, and nanoscale protrusions are less pronounced. Irrespective of the distance between the blind microholes, the melting effect is significant in both the cases. As the distance between the holes increased, a large presence of unprocessed alumina surface is visible. The huge amount of melting observed in the blind microholes can be related to the accumulation of thermal energy at a localized area (approximately 15 μm) due to the low thermal conductivity ($24 \text{ W m}^{-1} \text{ K}^{-1}$) and thermal expansion coefficient ($7.7 \times 10^{-6} \text{ K}^{-1}$) of Al_2O_3 .

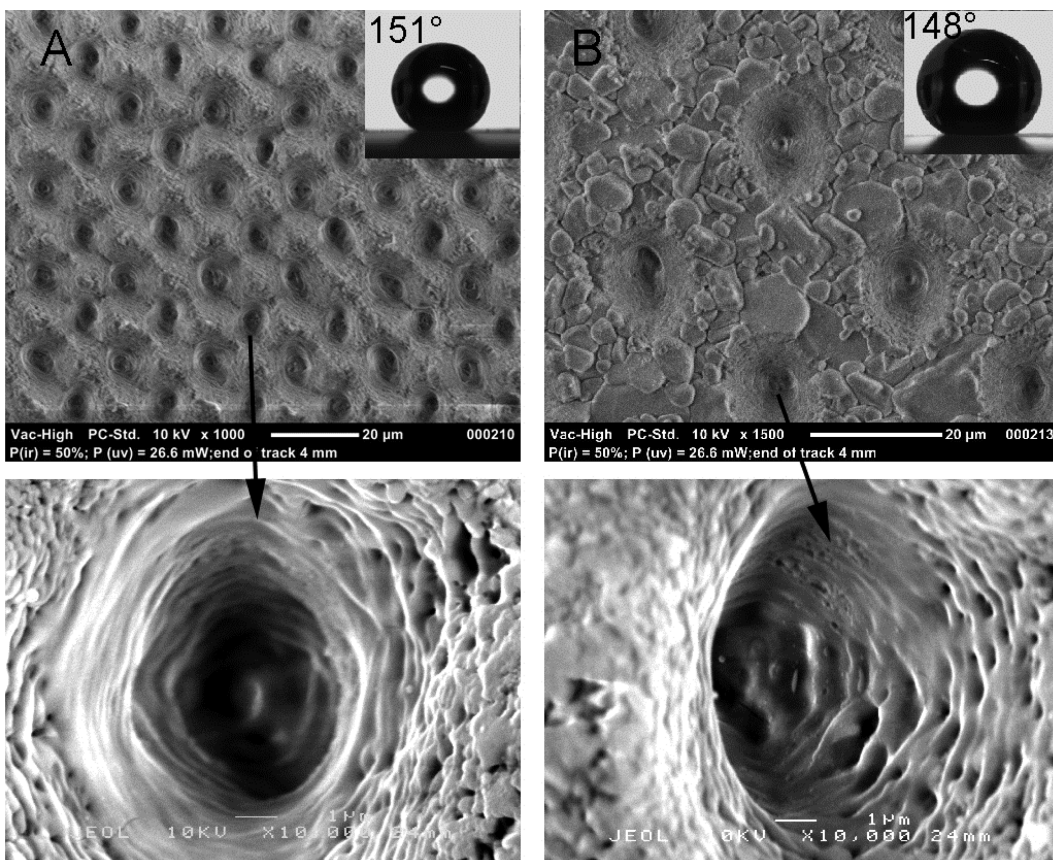


Figure 3. SEM pictures of laser-generated micropillars: (A) 375 pulses/unit area and (B) 750 pulses/unit area.

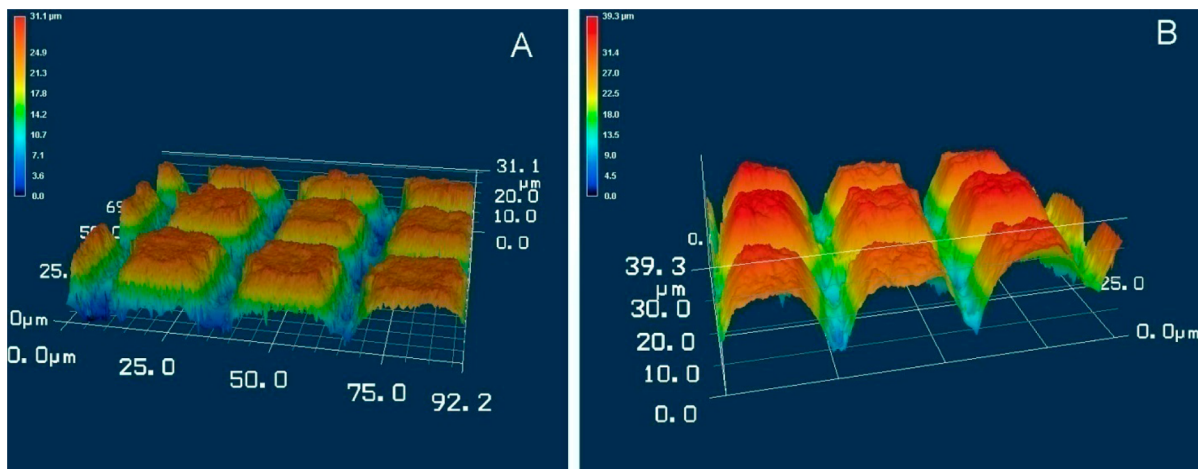


Figure 4. CLSM images of micropillars: (A) 375 pulses/unit area and (B) 750 pulses/unit area.

CLSM images of micropillars are shown in Figure 4. As the number of pulses/unit area varies, the height of the micropillars has also been increased. For the micropillars produced with 375 and 750 pulses/unit area, a maximum height of 31.1 and 39.9 µm, respectively, was recorded. Further, the channel width also increased for the micropillars processed with 750 pulses/unit area. As more and more laser pulses are applied at same spot, there can be a slight change in the diameter of the channel, due to application of more thermal energy to a localized area.

The bottom of the channel in between the pillars produced with 750 pulses/unit area appears relatively smooth compared to the micropillars produced with 375 pulses/unit area. This

could be attributed to the melt formation and resolidification during the laser processing.

The top edges of the micropillars are less sharp compared to the micropillars fabricated with fewer laser pulses. In summary, the area on the top surface of the micropillars is relatively less for the micropillars fabricated with 750 pulses/unit area. This reduction has been caused by the tail end of the Gaussian laser beam profile, which has very low energy density compared to the hat region of the Gaussian beam.

The effect of micropatterning on the wetting properties of the Al_2O_3 samples was evaluated by static sessile drop SCA measurements, using a droplet size of 8 µL. The plain Al_2O_3

surface recorded a SCA value of $60^\circ \pm 3^\circ$. The whole laser-patterned surface was highly hydrophilic within minutes of processing. The SCA measurements were unable to be computed due to very low CA values (less than 40°). However, the measurements performed after 24 h exhibited the hydrophobic character. The SCA recorded was in the range of 130° – 140° . The micropillars fabricated with 375 pulses/unit area showed consistency with respect to volume of the droplet size applied as well as repeated SCA measurements at the same spot. This sample exhibited superhydrophobicity even for a water droplet size of $12\ \mu\text{L}$. The other sample recorded a sharp decrease of more than 5° for the higher droplet size. Figure 5

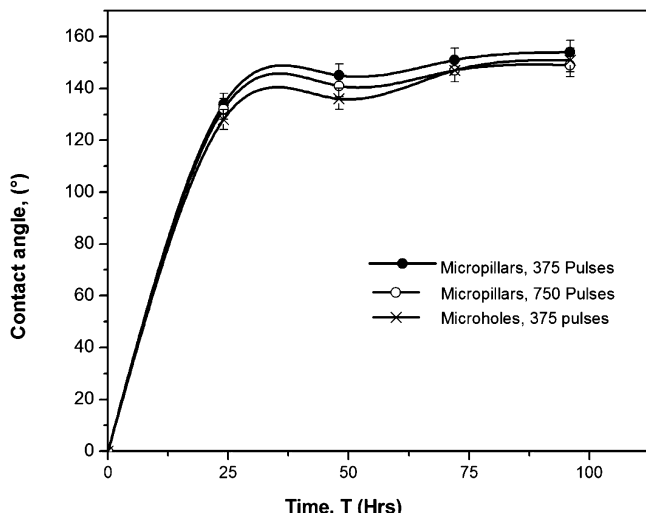


Figure 5. Static contact angle evaluation with respect to time for the micropillars and blind microholes.

represent the CA measurement as a function of time. Out of the two patterns, micropillars fabricated with 375 pulses/unit area showed promising results in terms of wetting properties. The relatively low pronouncement of CA measurements for the other samples may be related to geometrical differences.

In addition to the micromanipulation on the surface, it is essential to investigate the chemical changes on the laser-patterned surface, which is a key factor for the water repellency of the surface. Figure 6 shows the EDS spectrum recorded for plain Al_2O_3 sheets, blind microholes, and micropillars. Relatively large peaks are revealed at $\sim 1.4\text{ keV}$, corresponding to the $\text{K}\alpha$ absorption energies of Al.

The next large peak observed at $\sim 0.4\text{ keV}$ corresponds to oxygen. These two peaks are common in all the three spectra recorded. The computed elemental concentration is shown in Table 2. The atom percent of oxygen has been reduced in the laser-patterned Al_2O_3 samples from 62.22 atom % on plain surface to 55.43 atom % for the micropillars. The aluminum concentration has been increased from 37.77 atom % on plain surface to 43.64 atom % for the micropillars. The microholes have a lesser amount of Al on the surface compared to the micropillars. However, the chemical changes induced by laser-patterning of the alumina surface are not very significant compared to the micromanipulation.

4. DISCUSSION

The prime factor that promotes the laser micromachining with ultrashort laser pulses is the near-zero heat-affected zone or

cold processing. The diffusion depth “ l ” can be calculated by the following relationship

$$l = \sqrt[3]{k\tau_p} \quad (1)$$

where k is the thermal diffusivity of the material and τ_p is the pulse duration of the laser. Equation 1 clearly suggest that the shorter the laser pulse duration, the shorter the heat-affected zone, thus producing better machining precision. Eventually, the depth of the heat-affected zone could be minimized to be less than the optical skin depth, and hence, no thermal effect occurs.²¹ However, these arguments are contradicted in several experimental works reported.^{22,23} In our experiments, the melting effect is well-pronounced for the micropillars fabricated with 750 pulses/unit area and for the microholes generated with picosecond laser pulses. The melting effect was observed due to the localized pool of heat generated by the continuous application of train laser pulses at the same location and the low thermal conductivity of the Al_2O_3 . Moreover, the sample does not have redeposited material or debris on the surface. This cleanliness may be due to the low laser fluence (2.8 J/cm^2) used for the micromachining of the samples, which is very low compared to the threshold fluence required for particulate ejection.²⁴ The effect of melting is higher in blind microholes compared to the micropillars processed with same number of laser pulses, 375 pulses/unit area.

The laser-patterned samples exhibited superhydrophobicity without any additional coating or reactive gas environments during laser processing. The micromanipulated samples do not show any thermal cracks. The micropillars fabricated with 375 pulses/unit area showed a high degree of superhydrophobicity compared to other samples. On the surfaces with micropillars and microholes, the water droplets have contact with the top surface of the pillars, which creates an additional liquid/air interface compared to the solid/liquid interface on the plain samples. Moreover, micropillars fabricated with 375 pulses/unit area have nanoscale features on the top surfaces of the pillars. Therefore, the spacing between the nanoscale structures can be believed to be much smaller than the curvature of the meniscus, which has been caused by the gravitational force acting on the water droplet liquid interface. This compliments the consistency in hydrophobicity of the surface even for higher volume water droplets. This kind of nanoscale feature is not well formed on the sample treated with a higher number of pulses/unit area and microholes patterns due to the localized melting. Perhaps, the lack of nanoscale features may be the cause of the decrease in the CA values and the inconsistency of the hydrophobic property.

The heights of the micropillars are directly proportional to the number of laser pulses applied to the unit area. The increase in the height of the micropillars also increases the channel width or spacing between the micropillars, which provides easy passage for the water droplet to get into the channel and flush out the air trapped inside channels, thus reducing the static contact angle. The reduction in the SCA is very rapid when a bigger water droplet, such as $12\ \mu\text{L}$ and above, is applied.

EDS analysis shows a minor reduction of the oxygen present at the surface, and the reduction is directly proportional to the improvement in the wetting properties. However, for Al_2O_3 sample, the micropatterns play a major role in improving the wetting properties. The micropillars fabricated with 375 pulses/unit area recorded a high CA value of $153^\circ \pm 3^\circ$, and it is very consistent with a higher volume ($12\ \mu\text{L}$).

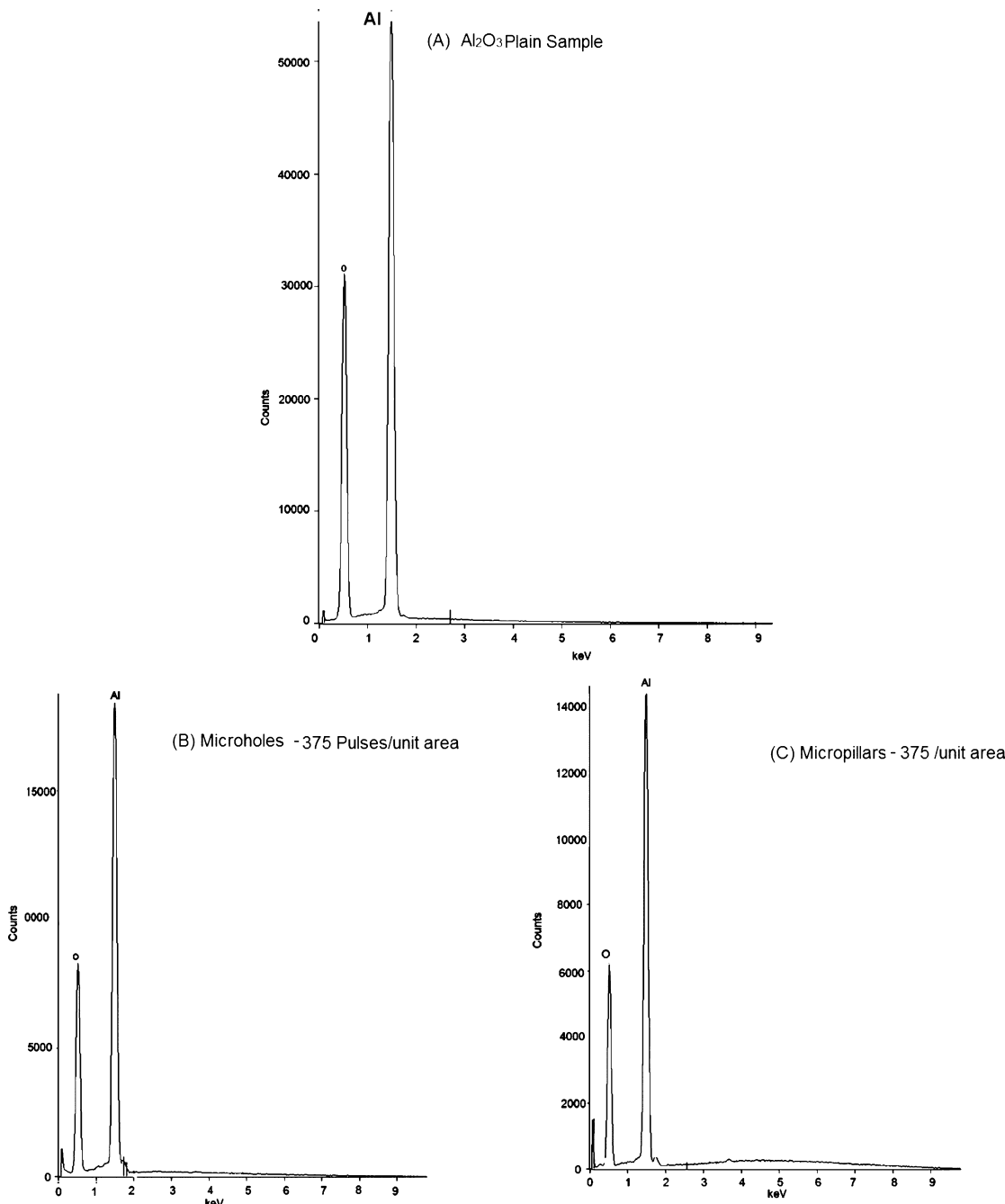


Figure 6. EDS spectrum recorded for plain Al₂O₃ (A) and laser-patterned microholes (B) and micropillars (C).

Table 2. EDS Measurement for the Micropatterns

sample	aluminum (atom %)	oxygen (atom %)
plain Al ₂ O ₃	37.77	62.22
microholes	41.39	58.61
micropillars	43.64	55.43

5. CONCLUSION

Thin sheets of alumina (Al₂O₃) are micromachined with ultraviolet laser pulses of 6.7 ps, to create a superhydrophobic surface with single-step processing. The impact of the number of pulses/unit area with respect to the geometry and static contact angle measurements has been investigated. The surface is free from cracks, and a melting effect is well-pronounced for the blind microhole structures, irrespective of the applied laser

pulses. The elemental analysis of the laser-patterned surface revealed a marginal change in its elemental composition. The amount of Al in the laser-patterned area has been increased in comparison with the unprocessed plain Al₂O₃ substrate. The results show that the micropatterns or geometry created by laser processing plays a major role rather than the chemical changes induced on the surface for improving the degree of hydrophobicity. Laser-processed micropillars exhibited a superhydrophobic surface with CA measurement of 150° ± 3°. The CA values are very consistent for a water droplet with an even bigger volume, such as 12 μL.

■ AUTHOR INFORMATION

Corresponding Author

*E-mail: rjagdheesh@yahoo.com.

Notes

The authors declare no competing financial interest.

ACKNOWLEDGMENTS

The author thanks Seetharam Mahadevan and Martyn Sherriff, School of Mechanical and Manufacturing Engineering, The University of New South Wales, for their technical support.

REFERENCES

- (1) Wolff, S.; Saxena, I. A preliminary study on the effect of external magnetic fields on laser-induced plasma micromachining (LIPMM). *Manuf. Lett.* **2014**, *2* (2), 54–59.
- (2) Torres-Péiro, S.; González-Ausejo, J.; Mendoza-Yero, O.; Mínguez-Vega, G.; Lancis, J. Femtosecond laser micromachining with extended depth of focus by using diffractive lenses. *Appl. Surf. Sci.* **2014**, *303*, 393–398.
- (3) Gupta, S.; Molian, P. Design of laser micromachined single crystal 6H-SiC diaphragms for high-temperature micro-electro-mechanical-system pressure sensors. *Mater. Des.* **2011**, *32*, 127–132.
- (4) Miwa, M.; Nakajima, A.; Fujishima, A.; Hashimoto, K.; Watanabe, T. Effects of the surface roughness on sliding angles of water droplets on superhydrophobic surfaces. *Langmuir* **2000**, *16*, 5754–5760.
- (5) Wenzel, R. N. Resistance of solid surfaces to wetting by water. *Ind. Eng. Chem.* **1936**, *28*, 988–994.
- (6) Jagdheesh, R.; Pathiraj, B.; Karatay, E.; Romer, G. R. B. E.; Huis in't Veld, A. J. Laser-induced nanoscale superhydrophobic structures on metal surfaces. *Langmuir* **2011**, *27*, 8464–8469.
- (7) Pan, Q.; Cheng, Y. Superhydrophobic surfaces based on dandelion-like ZnO microspheres. *Appl. Surf. Sci.* **2009**, *255*, 3904–3907.
- (8) Wang, Q.; Zhang, B.; Qu, M.; Zhang, J.; He, D. Fabrication of superhydrophobic surfaces on engineering material surfaces with stearic acid. *Appl. Surf. Sci.* **2008**, *254* (7), 2009–2012.
- (9) Sarkar, D. K.; Farzaneh, M.; Paynter, R. W. Superhydrophobic properties of ultrathin rf-sputtered Teflon films coated etched aluminum surfaces. *Mater. Lett.* **2008**, *62* (8–9), 1226–1229.
- (10) Long, J.; Fan, P.; Zhong, M.; Zhang, H.; Xie, Y.; Lin, C. Superhydrophobic and colorful copper surfaces fabricated by picosecond laser induced periodic nanostructures. *Appl. Surf. Sci.* **2014**, *311*, 461–467.
- (11) Krüger, J. r.; Kautek, W.; Lenzner, M.; Sartania, S.; Spielmann, C.; Krausz, F. Laser micromachining of barium aluminium borosilicate glass with pulse durations between 20 fs and 3 ps. *Appl. Surf. Sci.* **1998**, *127-129*, 892–898.
- (12) Semaltianos, N. G.; Perrie, W.; French, P.; Sharp, M.; Dearden, G.; Watkins, K. G. Femtosecond laser surface texturing of a nickel-based superalloy. *Appl. Surf. Sci.* **2008**, *255*, 2796–2802.
- (13) Pappas, D.; Bujanda, A.; Demaree, J. D.; Hirvonen, J. K.; Kosik, W.; Jensen, R.; McKnight, S. Surface modification of polyamide fibers and films using atmospheric plasmas. *Surf. Coat. Technol.* **2006**, *20* (1), 4384–4388.
- (14) Baldacchini, T.; Carey, J. E.; Zhou, M.; Mazur, E. Superhydrophobic surfaces prepared by microstructuring of silicon using a femtosecond laser. *Langmuir* **2006**, *22*, 4917–4919.
- (15) Zorba, V.; Stratakis, E.; Barberoglou, M.; Spanakis, E.; Tzanetakis, P.; Fotakis, C. Tailoring the wetting response of silicon surfaces via fs laser structuring. *Appl. Phys. A* **2008**, *93*, 819–825.
- (16) Bhattacharya, P.; Gohil, S.; Mazher, J.; Ghosh, S.; Ayyub, P. Universal, geometry-driven hydrophobic behaviour of bare metal nanowire clusters. *Nanotechnology* **2008**, *19*, 075709.
- (17) Kietzig, A.-M.; Hatzikiriakos, S. G.; Englezos, P. Patterned superhydrophobic metallic surfaces. *Langmuir* **2009**, *25* (8), 4821–4827.
- (18) Wu, B.; Zhou, M.; Li, J.; Ye, X.; Li, G.; Cai, L. Superhydrophobic surfaces fabricated by microstructuring of stainless steel using a femtosecond laser. *Appl. Surf. Sci.* **2009**, *256*, 61–66.
- (19) Cassie, A. B. D.; Baxter, S. Wettability of porous surfaces. *Trans. Faraday Soc.* **1944**, *40*, 546–551.
- (20) Kim, S. H.; Sohn, I.-B.; Jeong, S. Ablation characteristics of aluminum oxide and nitride ceramics during femtosecond laser micromachining. *Appl. Surf. Sci.* **2009**, *255*, 9717–9720.
- (21) Liu, X.; Du, D.; Mourou, G. Laser ablation and micromachining with ultrashort laser pulses. *IEEE J. Quantum Electron.* **1997**, *33*, 1706–1716.
- (22) Breitling, D.; Ruf, A.; Dausinger, F. Fundamental aspects in machining of metals with short and ultrashort laser pulses. *Proc. SPIE* **2004**, *5339*, 49–63.
- (23) Dausinger, F. Machining of metals with ultrashort laser pulses: From fundamental investigations to industrial applications. *Proc. SPIE* **2005**, *5777*, 840–845.
- (24) Mendes, M.; Vilar, R. Influence of the processing parameters on the formation and deposition of particles in UV pulsed laser ablation of Al₂O₃–TiC ceramics. *Appl. Surf. Sci.* **2003**, *217*, 149–162.